A DETAILED IMPACT RISK ASSESSMENT OF POSSIBLE PROTECTION ENHANCEMENTS TO TWO LEO SPACECRAFT

H. Stokes[(1)], C. Cougnet[(2)], M. David[(3)], J. Gelhaus[(4)], M. Röthlingshöfer[(5)]

[(1)] PHS Space Ltd, 8 Dixon Terrace, Pitlochry, PH16 5QX, UK. Email: hedley_stokes@msn.com
[(2)] EADS Astrium, 31402 Toulouse, France. Email: claude.cougnet@astrium.eads.net
[(3)] EADS Astrium, 88039 Friedrichshafen, Germany. Email: matthieu.david@astrium.eads.net
[(4)] Technische Universitaet Braunschweig, 38108 Braunschweig, Germany. Email: j.gelhaus@tu-bs.de
[(5)] EADS Astrium, 88039 Friedrichshafen, Germany. Email: mario.roethlingshoefer@astrium.eads.net

ABSTRACT

The SHIELD3 impact risk analysis tool has been used to compute the impact-induced probability of no failure (PNF) of two different spacecraft – a radar satellite and an optical satellite – operating in the 2020-2030 low Earth orbit debris environment. Based on this assessment, potential vulnerabilities were identified in the spacecraft designs, and several solutions were proposed for enhancing protection. The effectiveness of each shielding solution was determined by recalculating the spacecraft PNFs. Significant improvements in PNF were achieved, indicating that effective levels of extra protection can be implemented in spacecraft designs within constraints such as cost, mass and volume.

1 INTRODUCTION

The debris population in low Earth orbit (LEO) has increased significantly during the past decade. Consequently, the impact risk to high-value unmanned spacecraft operating in this region has also grown. It is becoming increasingly necessary, therefore, for manufacturers to consider assessing impact risk during the design of a spacecraft. Most of the available impact risk analysis models accomplish this by calculating the probability of no penetration (PNP) of the outer surfaces of a spacecraft. However, to obtain the probability of no failure (PNF) of a spacecraft, it is necessary to determine the potential damage to equipment if a particle penetrates inside the spacecraft. Thus, a higher fidelity analysis is required.

One software tool that has been specially designed for this purpose during the past 17 years is SHIELD3 [1, 2]. The software uses a variety of damage equations and debris cloud models to evaluate the damage to equipment from particles penetrating inside a spacecraft. This information is then combined with a failure model of the spacecraft to calculate its PNF. Recently the tool has been used within a European Commission FP7-funded project called ReVuS to analyse the designs of two different LEO spacecraft – one a radar satellite, the other an optical satellite – operating over the 2020-2030 timeframe [3]. Geometrical representations of both satellites were constructed in SHIELD3 and material properties assigned to each of their surfaces. Equipment redundancies and failure criteria were also defined. Debris and meteoroid fluxes from MASTER-2009 were then used to generate test particles in the SHIELD3 simulations. Results from the simulations were output in various forms, including: 3D geometrical displays of impact and penetration fluxes, tables of PNFs for groups of redundant equipment, and plots of satellite PNF versus impactor size. In summary, the analysis showed that the PNF of each satellite is relatively high.

To increase the PNFs of the satellites further, a range of possible shielding solutions were proposed for the most vulnerable areas. Three competing solutions were considered to be viable for the radar satellite and two for the optical satellite. These mainly involved various combinations of enhancements to multi-layer insulation and sandwich panels, and the relocation of some critical equipment items. The relative effectiveness of the five solutions was then quantified using SHIELD3 by recalculating the satellite PNFs. This paper presents the results of that analysis.

2 SHIELD3 IMPACT RISK ANALYSIS METHODOLOGY

To perform an impact risk assessment of a typical spacecraft design in SHIELD3 a 3D representation of the spacecraft is constructed. The geometry of the entire spacecraft structure, including external panels and internal walls and shelves, is modelled, and material properties are assigned to each of these structural elements. Each equipment item on the spacecraft is defined in terms of its geometry, material properties, function, redundancy, mission criticality, interfaces with other equipment, and location on the spacecraft.

For the next step in the methodology, the software simulates the impact and penetration distributions on the spacecraft. In SHIELD3, the impact distribution is derived by employing a Poisson routine to sample target-centered directional flux data generated by a debris environment model such as the ESA MASTER model. Test particles are then created and fired at the 3D geometry using a standard ray-trace method to find

Proc. '6th European Conference on Space Debris'
Darmstadt, Germany, 22–25 April 2013 (ESA SP-723, August 2013)

the precise impact points. Having obtained the impact distribution, appropriate ballistic limit equations (BLEs) are called up to ascertain which of the impacting particles penetrate external surfaces of the spacecraft structure or external equipment. In order to derive a statistically meaningful distribution of penetrating particles on the spacecraft geometry, the entire lifetime simulation is repeated many thousands of times. That is, a Monte Carlo simulation is performed. The result is a large distribution of penetrating particles. From this dataset, it is a straightforward matter to calculate the PNP of the external surfaces of the spacecraft.

In the final part of the methodology, the damage inside the spacecraft is assessed. SHIELD3 has a number of proprietary algorithms for analysing penetrative impact damage inside a spacecraft. The code also contains algorithms published in the open literature, such as the engineering fragmentation model described in [4], as well as a wide range of damage equations, including the SRL ballistic limit equation [5, 6]. Each of the particles that penetrates inside a spacecraft creates a secondary debris cloud that can interact with one or more equipment items, harnessing, and internal structures. A combination of ray-trace and geometrical methods is used to identify the intersection of the cloud with these interior elements. Depending on the configuration of the interaction, one of the damage assessment routines is utilized to determine which items are penetrated. For some scenarios a multi-wall BLE, such as the SRL equation, is suitable. However, for more complex scenarios, the interaction of individual elements of the cloud with internal surfaces is modelled.

The response of an equipment item to an impact is not simple. In some instances it is possible for a non-penetrative impact to cause an item to fail. Conversely, it is also possible that an item may survive a marginally penetrating impact, as was demonstrated in [7]. To cater for both of these cases, SHIELD3 samples failure probability profiles to determine whether each impacted item fails. In the event of an item failure, the consequences for the mission are determined using the reliability analysis module within SHIELD3. For example, if the equipment is not essential to the mission or has a redundant unit, then it is conceivable that the mission may continue largely unaffected. Essentially, mission success or failure is determined by the equipment's criticality and redundancy.

Finally, when each of the thousands of penetrative debris clouds has been analysed, the PNFs of individual equipment items (both internal and external) and groups of redundant items are calculated. Thus, the PNF of the whole spacecraft is calculated. This quantifies the impact survivability of the spacecraft design. Changes to the design, in terms of new protection solutions, can also be modelled and analysed in SHIELD3 by repeating the steps in the above process. SHIELD3 has been used in this way within the ReVuS project to demonstrate the survivability improvements that can be achieved by implementing a variety of different protection solutions in two different reference satellites.

3 ANALYSIS OF A RADAR SATELLITE

3.1 Input Data

Information on the baseline design of the radar satellite, including geometry data, material property data and reliability data, was supplied by EADS Astrium, Germany. Debris and meteoroid flux data was provided by the Technical University of Braunschweig, Germany. All of the data was input into SHIELD3 to build a representative model of the radar satellite.

The mission and orbit parameters used for the radar satellite are shown in Tab. 1.

Table 1. Mission and orbit parameters used for the radar satellite

Parameters	Data
Mission parameters:	
Start date	01/01/2020
End date	01/01/2030
Orbit parameters:	
Semi major axis (km)	6883.5
Eccentricity	0.1E-02
Inclination (degrees)	97.4
Right ascension of ascending node (degrees)	11.1
Argument of perigee (degrees)	90.0

Flux data from the ESA MASTER-2009 model was supplied in two files – one containing debris fluxes, the other containing meteoroid fluxes. The data format for both files was in accordance with the STENVI standard interface format as defined by the Inter Agency Space Debris Coordination Committee. The output spectrum for the flux data in both files is shown in Tab. 2.

Table 2. Output spectrum of the MASTER-2009 flux data files for the radar satellite

Parameter	Bin	Min	Max
Azimuth (degrees)	36	-180.0	+180.0
Elevation (degrees)	18	-90.0	+90.0
Velocity (km/s)	20	0.5	20.5
Diameter (m)	6	0.1E-04	0.1E+01
Latitude (degrees)	1	0.0	360.0
Density (g/cm^3)	10	0.0	10.0

Information on the configuration of the radar satellite, including the layout of its equipment, was provided in the form of an IGES file. Fig. 1 illustrates the level of detail supplied. Geometrical data was extracted from the IGES file and input into SHIELD3 to enable the same 3D representation to be reproduced.

The radar satellite bus is a hexagonal tube structure which is separated into three compartments by two

dividing walls. The majority of the bus structure is made from CFRP/Al sandwich panels and covered with multi-layer insulation (MLI). In Fig. 1 some of the external MLI and sandwich panels have been removed to enable internal equipment to be viewed.

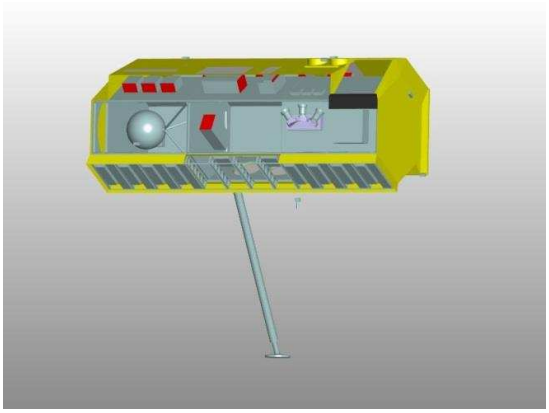

Figure 1. View of front and starboard sides of the radar satellite

Fig. 1 shows the interior of the rear and central compartments. Key items of the Attitude and Orbit Control Subsystem (AOCS), such as a titanium propellant tank, attitude control electronics, and magnetorquers, are housed inside these compartments. Most of the remaining subsystem equipment on the satellite is attached to various external surfaces of the hexagonal tube and is protected by an MLI tent comprising 7 layers of Mylar / Kapton. The radar payload, which is divided into 12 compartments comprising waveguides, TR modules and power conditioners, is also located on the outside of the hexagonal tube. Eight of the compartments are shown in Fig. 1 (with the covering waveguide panels removed). Note that the four compartments in the centre have been removed to enable two internal items to be seen more clearly. All 12 of the radar compartments are protected by a single layer of germanium MLI. Finally, there are a number of items located outside of the satellite bus structure and the MLI tent. These include Earth & sun sensors, S-band antennas, star tracker heads, an X-band boom and antenna, and a laser communication terminal.

3.2 Analysis of Baseline Design

Results of the SHIELD3 impact risk analysis of the baseline radar satellite design can be found in [8]. Therefore, only a brief summary will be presented here.

The flux of impactors in the size range 0.1 mm to 1.0 mm that penetrate the external surfaces of the radar satellite is shown on the 3D visualizations in Fig. 2. The surfaces with the highest penetration fluxes are coloured red, and those which experience the least penetrations are dark blue. One can see that the MLI tents protecting the equipment items at the top of the satellite, and the radar at the bottom (Earth-facing side) of the satellite, experience significantly more penetrations than those surfaces which are protected by a sandwich panel or a combination of sandwich panel and MLI. On the front face, the flux of penetrations through the MLI tent is ~8.9 penetrations / m^2 / year (coloured red in Fig. 2).

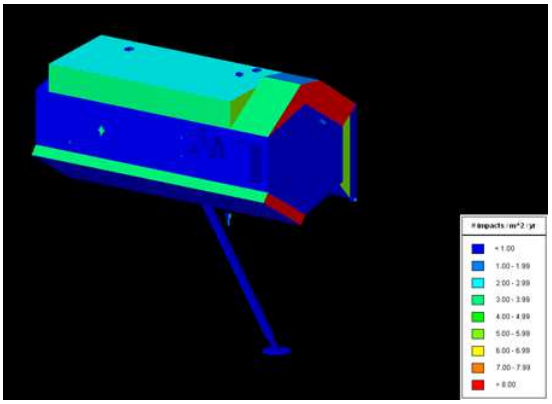

Figure 2. Flux of penetrators in the size range 0.1 – 1.0 mm on the radar satellite

To visualize how the penetration risk is distributed on the satellite, the number of penetrations on each equipment item is displayed in Fig. 3. Not surprisingly, exposed items such as the laser communication terminal and the star tracker assembly are the most vulnerable to penetration. Despite that, the overall PNF of the star tracker assembly is extremely high because of its 1-out-of-3 redundancy, and the laser communication terminal is not part of the risk assessment since it is a secondary payload. No other items stand out as being particularly vulnerable relative to the others, although the items which are protected only by the MLI tent have a higher penetration risk than those inside the hexagonal tube.

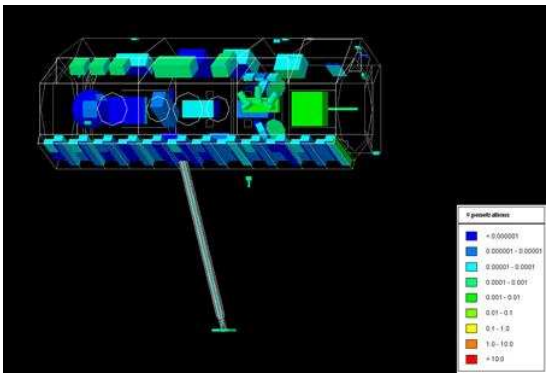

Figure 3. Number of penetrations of equipment on the radar satellite from 1.0 – 10.0 mm size particles

The impact failure risk of the radar satellite can be understood by plotting the probability of failure of the satellite as a function of impactor size. Results from the

SHIELD3 analysis are shown in Fig. 4. The graph reveals that sub-millimetre particles, although highly likely to impact the spacecraft, do not present a significant problem. That is, they are unlikely to cause sufficient damage to lead to a failure of the satellite. Conversely, large particles, e.g. > 1 cm, can do a lot of damage, but are unlikely to hit the satellite. Therefore, they also have a low probability of causing failure. However, between these extremes lies a region in which the combination of particle size and flux dominate the failure probability. This occurs in the size range 1 to 5 mm, with a peak at approximately 2 mm.

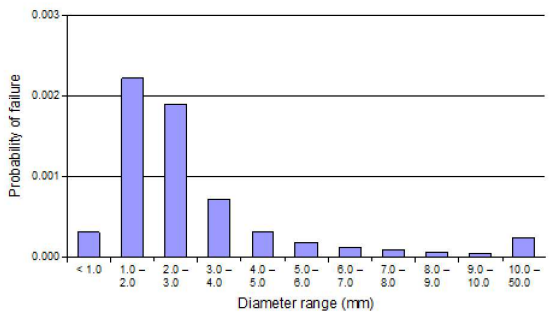

Figure 4. Radar satellite probability of failure due to impacts with particles in the size range 0 to 50 mm

The total PNF of the radar satellite across the entire impactor size range is ~0.994. One might judge this to be sufficiently high that there is no need to implement any additional protection measures. This is perhaps not surprising given the relatively benign debris environment in which the satellite will be operating, coupled with the fact that the satellite presents a fairly small cross-sectional area in the flight direction.

3.3 Description of Protection-Enhancements

Three different shielding solutions were proposed to increase the impact-related PNF of the radar satellite. In the first shielding solution one of the main enhancements was to the MLI tent surrounding many of the externally-mounted equipment items on the main hexagonal tube structure, as shown in Fig. 5. For those parts of the MLI tent that perform a radiator function, CFRP plates were placed under the MLI (i.e. the dark areas in the figure). For the non-radiator parts of the MLI, two layers of stainless steel mesh were added. These are shown by the light brown areas in the figure.

In the first shielding solution, enhancements were also made to critical equipment items which were identified as being the most vulnerable during the analysis of the baseline design, i.e. units protected only by the MLI tent. Parts of the aluminium casing around these units were thickened so that the total ballistic limit of the enhanced MLI tent + thickened unit casing was at least 3 mm.

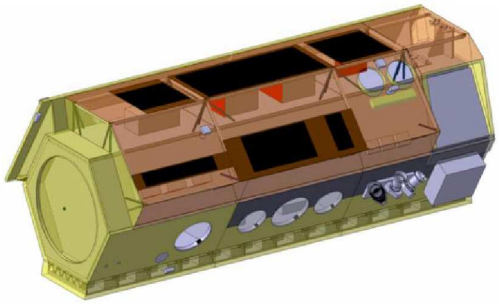

Figure 5. Shielding enhancements to the MLI tent on the radar satellite (shielding solution #1)

In the second shielding solution, the proposed enhancements focused on the same parts of the satellite as those for shielding solution #1. However, for this solution, CFRP sandwich panels were placed under the MLI tent radiator areas instead of CFRP plates, as shown by the dark areas in the figure. Also, the remaining non-radiator tent area was protected by two MLI blankets separated by 20 mm; the inner MLI was reinforced with a Nextel sheet and the outer MLI with two layers of stainless steel mesh. Vulnerable surfaces of critical equipment items were also thickened. Again, the combination of MLI tent and unit casing protection was designed to increase the ballistic limit of these items to at least 3 mm.

The third shielding solution was similar in many respects to the first. The main difference between shielding solution #3 and shielding solution #1 concerned the relocation of some critical equipment units inside the hexagonal tube structure of the satellite. The CFRP sandwich panels protecting these relocated items also had their face-sheets thickened. As before, the goal was to reach a 3 mm ballistic limit.

3.4 Analysis of Protection-Enhanced Design

Each of the three proposed shielding solutions were implemented in the SHIELD3 model of the baseline radar satellite design and analysed in turn. The resulting PNFs are listed in Tab. 3. It can be seen that the PNFs of all three solutions are significantly higher than the value obtained for the baseline design. During the definition of the shielding solutions a notional PNF requirement of 0.997 was specified, which was estimated to be achievable based on a ballistic limit of 3 mm for the protection-enhanced items. Thus, all three shielding solutions have exceeded this requirement.

Table 3. PNF data for each of the radar satellite shielding solutions

Description	PNF
Baseline design	0.99377
Shielding solution #1	0.99845
Shielding solution #2	0.99875
Shielding solution #3	0.99885

To understand the impact failure risks, it is instructive to reproduce the graph in Fig. 4, but with the results for the three shielding solutions also plotted, as shown in Fig. 6. It is clear that there is still a peak in the 1.0 – 2.0 mm particle size range, however the size of the peak is much smaller for each of the shielding solutions. Thus, the shielding solutions are effective in preventing many of the 1.0 – 5.0 mm size particles from terminating the mission. That said, the graph also reveals that particles in the size range 1 mm to 1 cm remain the dominant impact failure risk, irrespective of which shielding solution is applied.

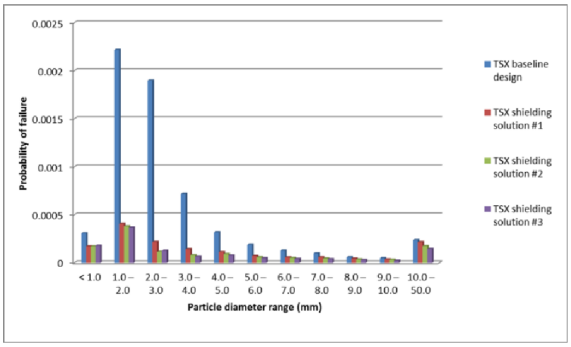

Figure 6. Failure probability vs. impactor size for each of the radar satellite shielding solutions

Finally, Fig. 7 shows a plot of the probability of penetration of the most critical items in the baseline design and in the three shielding solutions. It can be seen that the penetration probabilities are almost an order of magnitude lower with shielding applied.

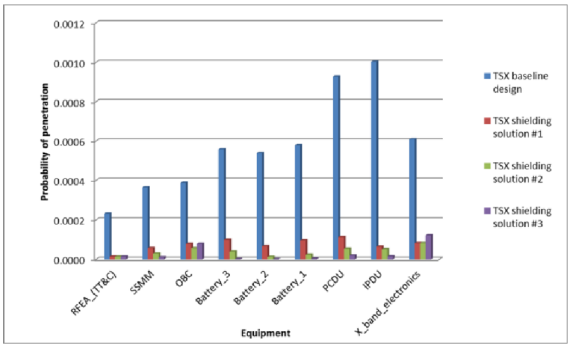

Figure 7. Penetration probability of critical equipment for each of the radar satellite shielding solutions

4 ANALYSIS OF AN OPTICAL SATELLITE

4.1 Input Data

Information on the baseline design of the optical satellite was supplied by EADS Astrium, France. As before, debris and meteoroid flux data was provided by the Technical University of Braunschweig, Germany. All of the data was input into SHIELD3 to build a representative model of the optical satellite.

The mission and orbit parameters used for the optical satellite are shown in Tab. 4.

Table 4. Mission and orbit parameters used for the optical satellite

Parameters	Data
Mission parameters:	
Start date	01/01/2020
End date	01/01/2030
Orbit parameters:	
Semi major axis (km)	7200.6
Eccentricity	0.1E-02
Inclination (degrees)	98.7
Right ascension of ascending node (degrees)	0.0
Argument of perigee (degrees)	0.0

The debris and meteoroid flux data files generated using MASTER-2009 were supplied in the STENVI interface format according to the same output spectrum as was used for the radar satellite (see Tab. 2). Data on the satellite configuration was extracted from an IGES file and input into SHIELD3 to enable the same 3D representation to be reproduced. Views of the exterior and interior of the satellite are shown in Figs. 8 and 9.

Fig. 8 shows the orientation of the satellite relative to the flight direction and the Earth direction. The satellite comprises two identical optical systems mounted on top of a stack of three compartments, which are identified as follows: the Case compartment, which sits underneath the optics, the mid-section compartment, and the Service Module (SM), which is located at the bottom of the stack.

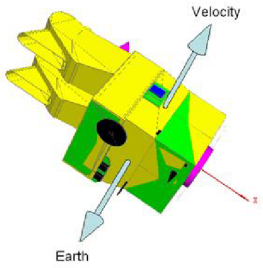

Figure 8. View of Earth and front facing sides of the optical satellite (excluding solar array)

Fig. 9 illustrates the positions of the individual equipment units inside the SM and the mid-section. These units provide a range of typical functions on a satellite, including on-board computing, attitude / orbit control, power distribution / regulation, and communications. A structural tube, known as the MDS, is located at the centre of the SM. A second tube, the MP, sits directly above the MDS tube within the mid-

section. The tubes house four batteries and two propellant tanks. Note that the four side panels around the mid-section are not shown in Fig. 9.

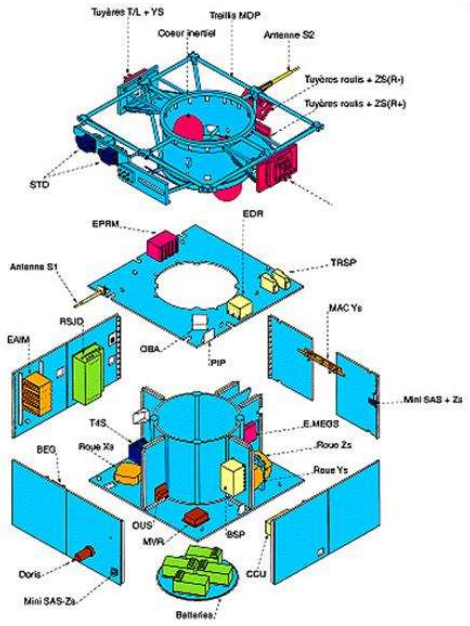

Figure 9. Exploded view of the optical satellite Service Module and mid-section

Equipment units located inside the Case compartment are used for controlling the two optical systems, and processing and transmitting the resulting images. The Case compartment walls are constructed using a combination of aluminium sandwich panel, CFRP/Al sandwich panels, and MLI walls.

In the Service Module, aluminium honeycomb sandwich panels are used throughout, and many of the sandwich panels are covered with MLI. The mid-section compartment (i.e. in-between the Case compartment and the Service Module) is protected by four walls made from MLI. Finally, the two optical systems are protected within a baffle + helmet compartment made from thin aluminium sheeting.

4.2 Analysis of Baseline Design

Results of the SHIELD3 impact risk analysis of the baseline optical satellite design can be found in [8]. Therefore, only a brief summary will be presented here.

The flux of penetrations on external surfaces from impactors in the size range 0.1 mm to 1.0 mm is shown in Fig. 10. It is immediately apparent that the front-facing walls of the Case compartment and the mid-section compartment, which are both made entirely from MLI, experience much higher penetration fluxes than the front-facing side of the Service Module, which is protected by a combination of aluminium honeycomb sandwich panels and MLI. For example, the flux of penetrations through the Case compartment MLI wall on the front face is ~41 penetrations / m^2 / year (coloured red in Fig. 10).

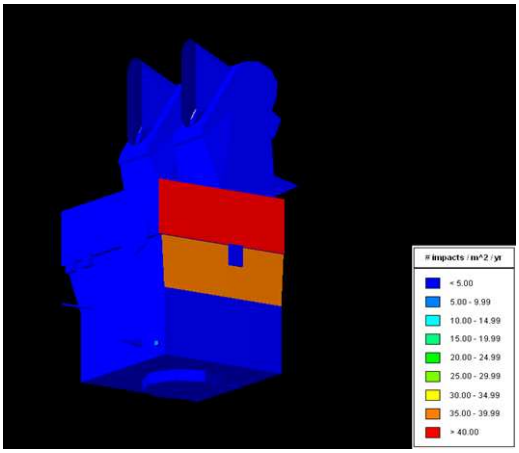

Figure 10. Flux of penetrators in the size range 0.1 – 1.0 mm on the optical satellite

To visualize the relative vulnerability of equipment inside the optical satellite, the number of penetrations on each equipment item is displayed in Fig. 11.

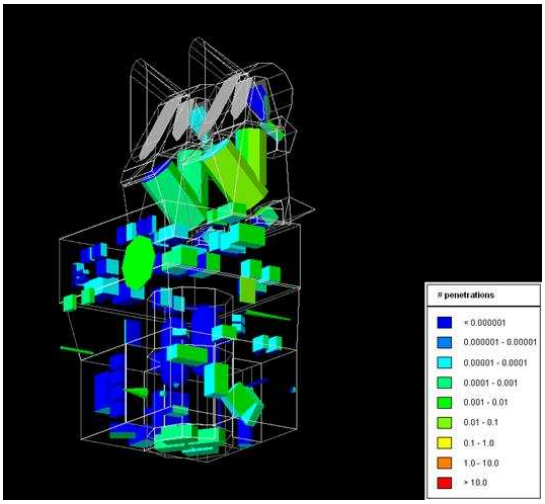

Figure 11. Number of penetrators of optical satellite equipment in the size range 1.0 – 10.0 mm

This figure shows the number of impactors that have sufficient energy to penetrate through the combination of external spacecraft wall and internal equipment casing. It is clear that those items closest to the flight direction suffer the greatest number of penetrations. In particular, the following items are the most vulnerable: two batteries, a computer, a pyrotechnics box, a reaction wheel, the EDR, and several electronics boxes in the Case compartment. Therefore, these items might be expected to dominate the computation of the satellite's

overall impact-induced PNF. With the exception of most of the Case equipment, which have distributed redundancy, this is true. Therefore, these items could be considered a priority for protection enhancement.

To understand the impact failure risk of the optical satellite, Fig. 12 shows a plot of the probability of failure of the satellite as a function of impactor size. As with the analysis of the radar satellite, the graph reveals that sub-millimetre particles, although highly likely to impact the spacecraft, are unlikely to cause a mission-terminating failure. Conversely, large particles, e.g. > 1 cm, can do a lot of damage, but are unlikely to hit the satellite. Therefore, they also have a low probability of causing failure. However, in-between these regions, the flux and size of particles are such that they dominate the failure probability. The graph reveals that particles in the size range 1.0 – 10.0 mm are responsible for the biggest drop in the satellite's impact-induced PNF. The peak of the impact failure risk occurs at around 2.5 mm.

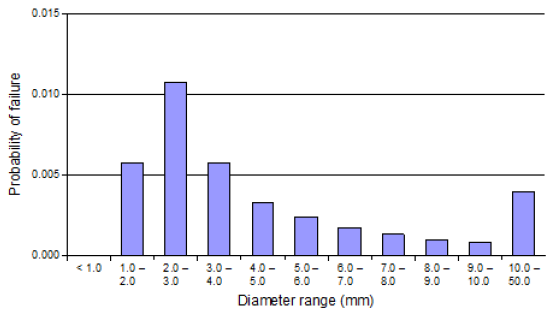

Figure 12. Optical satellite probability of failure due to impacts with particles in the size range 0 to 50 mm

The total PNF of the optical satellite across the entire size range is ~0.964. Although this is reasonably high, it was considered worthwhile to explore some shielding options for enhancing the satellite's impact protection.

4.3 Description of Protection-Enhancements

Two different shielding solutions were proposed to increase the impact-related PNF of the optical satellite. In the first shielding solution a number of different protection enhancements were made to surfaces facing the flight direction. These changes were designed to improve the survivability of critical equipment in the SM, mid-section compartment and Case compartment. In particular, some of the MLI blankets were reinforced with two layers of stainless steel mesh, as depicted by the light blue area in Fig. 13. Radiators within the MLI, shown as light brown rectangular, were also enhanced – in this instance with 0.2 mm thick CFRP sheets.

Enhancements were also made to vulnerable surfaces of critical equipment facing the flight direction. In particular, the dark blue surfaces were thickened by 3.7 mm. The surfaces coloured dark green, light green and red were also thickened, but by different amounts. An SM sandwich panel (coloured yellow) was also enhanced by increasing the thickness of its face-sheets. Finally, the four batteries were given extra protection by being moved up 200 mm so that they were totally inside the spacecraft structure.

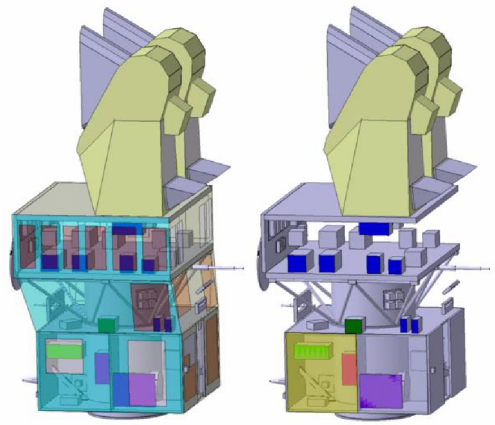

Figure 13. Two views of shielding enhancements on the optical satellite (shielding solution #1)

The protection enhancements in shielding solution #2 were similar to those in shielding solution #1, but with several notable differences. In particular, the enhanced MLI protecting the mid-section and Case compartments comprised two blankets. The outer blanket was enhanced with two layers of stainless steel mesh, whereas the inner blanket had an additional layer of Nextel. Within the MLI blankets, the rectangular radiator areas were reinforced with 20 mm thick CFRP sandwich panels behind them. For the critical equipment with dark blue coloured surfaces, protection was provided by the addition of a 20 mm aluminium sandwich panel. Other critical units were protected by an outer aluminium foam panel with a 20 mm thick aluminium sandwich panel behind.

It was expected that the protection improvements in both shielding solutions would increase the ballistic limit of the vulnerable flight-direction facing surfaces of the critical units to at least 3 mm.

4.4 Analysis of Protection-Enhanced Design

Both of the proposed shielding solutions were implemented in the SHIELD3 model of the baseline optical satellite design and analysed in turn. The resulting PNFs are listed in Tab. 5. Not surprisingly the PNFs of both solutions are somewhat higher than that obtained for the baseline design. During the definition of the shielding solutions a notional PNF requirement of 0.98 was specified, which was estimated to be achievable based on a ballistic limit of 3 mm for the protection-enhanced items. Thus, both shielding solutions have almost met this requirement.

Table 5. PNF data for both of the optical satellite shielding solutions

Description	PNF
Baseline design	0.96367
Shielding solution #1	0.97828
Shielding solution #2	0.97887

To understand the impact failure risks, it is instructive to reproduce the graph in Fig. 12, but with the results for the two shielding solutions also plotted, as shown in Fig. 14. It is clear that there is still a peak in the 2.0 – 3.0 mm particle size range; however the size of the peak is much smaller for the two shielding solutions. Thus, both solutions are effective in preventing many of the 1.0 – 5.0 mm size particles from terminating the mission. That said, the graph also reveals that particles in the size range 1 mm to 1 cm remain the dominant impact failure risk, irrespective of which shielding solution is applied.

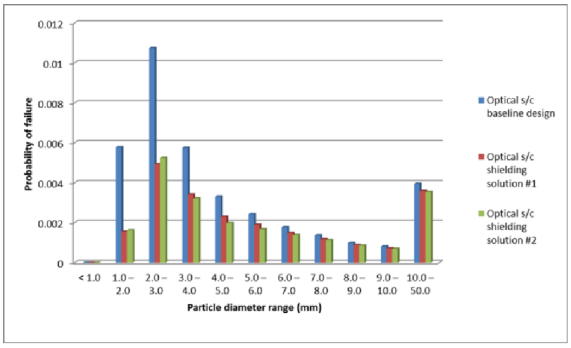

Figure 14. Failure probability vs. impactor size for each of the optical satellite shielding solutions

Finally, Fig. 15 shows a plot of the probability of penetration of the most critical items in the baseline design and in the two shielding solutions. It can be seen that the penetration probabilities for many of the items drop by at least a factor of two when shielding is applied. The most significant risk improvement comes from moving the two most vulnerable batteries deeper inside the spacecraft.

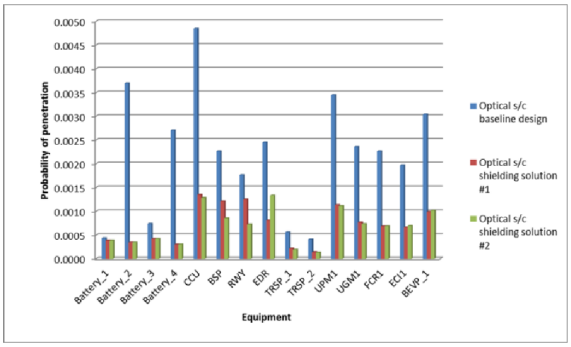

Figure 15. Penetration probability of critical equipment for each of the optical satellite shielding solutions

5 CONCLUSIONS

Within the framework of an EC-funded project called ReVuS, the probability of no failure (PNF) of two LEO spacecraft – one a radar satellite, the other an optical satellite – was computed using the SHIELD3 impact risk analysis software. Various shielding solutions were then applied to the satellites and the PNFs recalculated. Results showed that each solution could achieve a significant improvement in PNF. For the radar satellite, the PNF requirement was exceeded; however for the optical satellite the PNF requirement was not quite met. The results provide confidence that effective levels of extra protection can be implemented in spacecraft designs within the constraints of cost, mass and volume.

6 ACKNOWLEDGEMENTS

The authors wish to express their gratitude to the European Commission for funding this work under the Seventh Framework Programme (FP7).

7 REFERENCES

1. Stokes, P.H. & Swinerd, G.G. (2004). The Implementation of Cost Effective Debris Protection in Unmanned Spacecraft. *Adv. Space Res.* **34**, 1090-1096.

2. Stokes, P.H. & Swinerd, G.G. (2005). Debris Protection Optimisation of a Realistic Unmanned Spacecraft using SHIELD. *Proc. 4th Eur. Conf. Space Debris*, European Space Agency (ESOC), Darmstadt, Germany.

3. Cougnet, C., et al. (2013). Reducing the Vulnerability of Space Systems to Small Debris Particles. *Proc. 6th Eur. Conf. Space Debris*, European Space Agency (ESOC), Darmstadt, Germany.

4. Schäfer, F. (2006). An Engineering Fragmentation Model for the Impact of Spherical Projectiles on Thin Metallic Plates. *Intl. J. Impact Eng.* **33**, 745-762.

5. Schäfer, F., et al. (2008). Ballistic Limit Equation for Equipment Placed Behind Satellite Structure Walls. *Intl. J. Impact Eng.* **35**, 1784-1791.

6. Ryan, S., et al. (2008). A Ballistic Limit Equation for Hypervelocity Impacts on CFRP/Al HC Satellite Structures. *Adv. Space Res.* **41**, 1152-1166.

7. Putzar, R., et al. (2006). *Vulnerability of Spacecraft Equipment to Space Debris and Meteoroid Impacts*. Final report. Technical note No. 5 (TN5), ESA contract 16483/02. EMI-No. I-15/06.

8. Stokes, H., et al. (2012). A Detailed Impact Risk Assessment of Two Low Earth Orbiting Satellites. *Presented at 63rd Int'l Astronautical Congress, Naples, Italy*, IAC-12-A6.3.2.